APTEFF, 51, 1-206 (2020) UDC: 693.9:669.713:629.33]:639.45+679.92
DOI: https://doi.org/10.2298/APT2051163K BIBLID: 1450-7188 (2020) 51, 163-180
BY-NC-ND
Original scientific paper

INFLUENCE OF CALCINED SNAIL SHELL PARTICULATES ON MECHANICAL PROPERTIES OF RECYCLED ALUMINIUM ALLOY FOR AUTOMOTIVE APPLICATION

M.Y. Kolawole[1], J.O. Aweda[2], S. AbdulKareem[2], S.A. Bello[3], A. Ali[4], F. Iqbal[4]*

[1] Department of Mechanical Engineering, Faaculty of Engineering and Technology, Kwara State University Malete, Nigeria
[2] Department of Mechanical Engineering, Faaculty of Engineering and Technology, University of Ilorin, Ilorin, Nigeria
[3] Department of Materials Science and Engineering, Faaculty of Engineering and Technology, Kwara State University Malete, Nigeria
[4] Interdisciplinary Research Centre on Biomedical Materials, COMSATS University Islamabad, Lahore Campus, Pakistan

Nowadays, low-cost particulate reinforced metal matrix composites with improve mechanical properties are highly sought in various industrial and critical engineering applications including automotive and aerospace sectors. Meanwhile, increasing consumption rate of African giant land snail (Archachatina marginata) had been posing disposal challenges of its shells. Therefore, this paper tends to investigates the influence of waste snail shells particulates on the physical and mechanical properties of recycled aluminum-silicon alloy matrix. Different weight proportions i.e. (0 – 7.5) wt% of calcined snail shell particles at an interval of 1.5 wt% were successfully incorporated into Al-Si alloy matrix melted at 750 °C using stir-casting route. The microstructure, physical and mechanical properties of the resulting composites were examined and presented. Microstructural examination shows fairly uniform dispersion of snail shell particles in the aluminium alloy matrix intermingled with aluminium-silicon dendrites. Mechanical properties such as hardness, impact, compressive and tensile strengths increased with increasing addition of calcined snail shell particulate up to 6 wt% while density and elongation decreases. The total equivalent density reduction of 5.4% in composites compared to unreinforced alloy was obtained at 7.5 wt% snail shell addition. The maximum hardness, impact, compressive and tensile strengths obtained are 118±4 HV, 88 J, 552±20 MPa and 211 ± 4.8 MPa equivalent to 21, 25, 19 and 36 percent increase respectively relative to un-reinforced aluminium-silicon alloy. Hence, mechanical and physical properties of Al-Si alloy can be enhanced using calcined snail shell particulates which can widen its application in automotive industries.

Keywords: metal marix composite, low-cost reinforcement, mechanical properties, stir-casting, automotive and aluminium alloy

INTRODUCTION

The demand for light weight and cost-effective engineering materials with higher strength especially in automotive, aerospace and structural applications for enhance performance are on the increase (1, 2). Interestingly, aluminium and its alloys with matching

* Corresponding author: M.Y. Kolawole, Department of Mechanical Engineering, Faaculty of Engineering and Technology, Kwara State University Malete, Nigeria, e-mail: maruf.kolawole@kwasu.edu.ng

APTEFF, 51, 1-206 (2020) UDC: 693.9:669.713:629.33]:639.45+679.92
DOI: https://doi.org/10.2298/APT2051163K BIBLID: 1450-7188 (2020) 51, 163-180
BY-NC-ND
Original scientific paper

characteristics of light weight, low cost, good thermal and electrical properties desirable in various engineering applications had stimulated research interest. These overwhelming properties as well as the recyclability of aluminium had made it a promising candidate material of the present century in engineering applications. Moreover, good resistance to corrosion has further preserved the integrity of aluminium and its alloys' properties for improved performance in many environments. Barely all sectors of human endeavour today including and not limited to cooking utensils, household furniture, electrical industries, aerospace, automobile and structural applications are making use of aluminium either in their pure or and alloyed forms. However, global increasing demand for lightweight material with enhance mechanical properties over the conventional alloys in the emerging industrial applications and requirements has recently fuelled the curiosity of researchers on advanced engineering materials (metal matrix composites) developments (3, 4). Reinforcing a metal matrix phase resulted in metal matrix composite with processing techniques serving as major hub for tailoring the resulting properties into desired application. By literature search (5), research birth in metal matrix composites (MMCs) was dated back to about two decades ago. Interestingly, this has transpired into modern days advanced materials finding application in structural, aerospace, automotive, marine, electronic, wear and thermal applications. This was due to improved physical, mechanical properties and weight savings advantage associated with metal matrix composite compared to unreinforced alloys (6, 7).

Reinforcement materials can simply be regarded as strength enhancer or load carrying member in MMCs. It is usually a non-metallic in nature including ceramics, agro and bioshell wastes. It can also be classified according to its geometry into, continuous and discontinuous fibre, wiskers or particulate reinforcement materials (8). Literature has shown (9) that the mechanical properties of MMCs with continuous fibre has superior strength compered to whisker or particulate reinforced composites. However, particulate metal matrix composites (PMMCs) are easier to process, cost-effective with good isotropic properties advantages which could be automated (4, 10). In addition, properties of PMMCs can easily be processed for desirable applications by modifying the parameters thereof such as the particle size, volume fraction, stirring speed and time, melt temperature and solidification rate. As a result, synthetic reinforcement particles such as silicon carbide (SiC), alumina (Al_2O_3) are the earlier and mostly investigated in MMCs. However, their use in industrial production of MMCs had greatly been hindered by the scarce and increasing cost of synthetic reinforcement materials like alumina, silica oxide and silica carbide. As a result, modern day researches on material development are now exploring the use of industrial and agro allied waste products as a cost-effective and potential source of reinforcement materials in MMCs production (4, 6, 11). Various viable industrial and agro-wastes that had been investigated in aluminium alloy matrix include agricultural (rice husk, bamboo leaves, coconut shells and fibers, maize corb and husk, egg shells) wastes and industrial (fly ash, red mud) wastes materials (5, 12-19). Their findings revealed that agro and industrial wastes can be use as aluminium matrix reinforcement materials due to their promising properties enhancement.

African giant land snail shells (*Archachatina marginata*) is a bio-waste material readily available in Nigeria and other tropical regions of the world. However, their increasing consumption of its flesh due to medicinal benefit especially in Nigeria has been re-

APTEFF, 51, 1-206 (2020) UDC: 693.9:669.713:629.33]:639.45+679.92
DOI: https://doi.org/10.2298/APT2051163K BIBLID: 1450-7188 (2020) 51, 163-180
BY-NC-ND
Original scientific paper

sulting into indiscriminate disposal with associated environmental threats (4, 20, 21). But a recent study (4) of this species of snail shell confirmed the presence of ceramics phases with promising potentials to be use as low-cost metal matrix reinforcement material. Various available processing routes for processing of MMCs include squeeze casting, infiltration, powder metallurgy and stir casting techniques. However, stir casting process has widely been reported to be the most viable and economical route for particle reinforced metal matrix composites (PMMCs) processing and production (22). Moreover, its simplicity, cheap and applicability for large scale industrial production has made it to surpassed other fabrication routes (23, 24). Hence in this paper, Physical and mechanical properties of *Archchatina marginata* snail shell particulate reinforced aluminium-silicon alloy are presented.

MATERIALS AND METHODS

Materials used in this work are piston scraps made of aluminium-silicon alloy as matrix material and discarded African giant land snail shells as reinforcement materials.

Processing of matrix materials

The scraps of aluminium piston sourced from Ipata-Oloje mechanic market in Ilorin, Kwara State, Nigeria was used in this study. The collected piston scraps were washed with detergents and warm water to obtain a clean and oily free aluminium scrap. It was then sun dried for three days before melted in pit furnace and de-slagged three times to eliminate the impurities. The chemical composition of processed aluminium scrap used in this study as examined with SEM/EDX analysis is presented in Table 1.

Table 1: Elemental composition of Al-Si alloy

Elements	Al	Si	C	O	Na	Br	Sr
Wt% Composition	87.10 ± 1.500	7.70 ± 0.950	0.03 ± 0.001	4.95 ± 0.250	0.01 ± 0.005	0.18 ± 0.002	0.03 ± 0.001

Reinforcement materials preparation and characterization

Figures 1 (a & b) shows the photograph of the *Archachatina Marginata* snail shells (SnS_p) and its powder form as used in this study. The elemental composition (by weight) of snail shell had previously been reported to contains 81% calcium carbonate in addition to other elements like silicon, aluminium, Sulphur, bromine, tin and potassium (4). The cleaned and dried snail shells were crushed into powder via a disc mill and subjected to calcination at 900 °C for 3 hours to obtain a thermally stable reinforcement material. The resulting powder obtained from calcination was followed by sieving analysis using BS1377:1990 standard procedure. The sieve sizes were arranged in descending order of fineness (250, 200, 150 and 100 μm). The powder retained at 100 μm sieve size was used in this work. The functional group analysis of both calcined and un-calcined S_nS_p inspected using Thermo-Nicolet 6700P FTIR Spectrometer (USA) in the range of 4000 cm^{-1} to 500 cm^{-1} using Attenuated Total Reflectance (Smart iTR) mode. Determination of SnS_p

APTEFF, 51, 1-206 (2020) UDC: 693.9:669.713:629.33]:639.45+679.92
DOI: https://doi.org/10.2298/APT2051163K BIBLID: 1450-7188 (2020) 51, 163-180
BY-NC-ND
Original scientific paper

(calcined and un-calcined) phase analysis was investigated using Cu-Kα (1.54 Å) radiations using PANalytical X'Pert Powder X-ray diffractometer from Philips, Netherlands. The diffractograms selected span through the range of 20 and 80° with step size of 0.02° and count time of 1 s per step. In addition, the morphology and particle size of the selected calcined snail shell powder (100 μm) was determined using SEM image supported with Microsoft word and Gwyddion 2.31. Resolution of SEM image as determined by Microsoft word is 0.91inches which is equivalent to 1 μm in the image. This scale was then used to determine the width (5.50 μm) and height (5.51 μm) of the SEM image which were used as impute data for width and height in the Gwyddion software for determining the particle sizes.



(a) (b)

Figure 1. Pictures of (a) Snail shell and (b) Snail shell powder.

Aluminium-silicon alloy/SnS_p composite production

Figure 2 shows the illustrative sketch of the stir-casting process used for the production of Al-Si alloy/xSnS_p matrix composite. Required amount of Al-Si alloy was kept in crucible which was first preheated to a red-hot condition in Thermo Scientific™ FD1340M electric muffle furnance before subsequently raising the temperature to 750 °C at 10 °C/min heating rate. Thereafter, 0.1 wt% of magnesium ribbon was added to the molten aluminum to enhance wettability (12, 25). 1.5 wt% 100 μm of calcined snail shell powders were preheated at 400 °C to increase its wettability and prevent hydrogen gas inclusion in the melt through absorption of moisture (OH^-) (26). The liquid Al-Si alloy at 750 °C was poured into a preheated graphite crucible and incorporate the preheated calcined snail shell particulates into the melt followed by manual stirring for 5 minutes. The slurry mixture was then placed in locally fabricated electric stirrer set-up with attached heat source and type K- thermocouple for temperature monitoring (Figure 2). The molten composite slurry at 750±10 °C was then stirred at 400 rpm for 120 s and finally poured into ϕ20 mm cavity of 150 mm height steel die. The same procedure was followed for 3, 4.5, 6 and 7.5 wt% of SnS_p additions in aluminium-silicon alloy matrix. The solidified Al-Si/xSnS_p composites were then subjected to mechanical properties test.

APTEFF, 51, 1-206 (2020) UDC: 693.9:669.713:629.33]:639.45+679.92
DOI: https://doi.org/10.2298/APT2051163K BIBLID: 1450-7188 (2020) 51, 163-180
BY-NC-ND
Original scientific paper

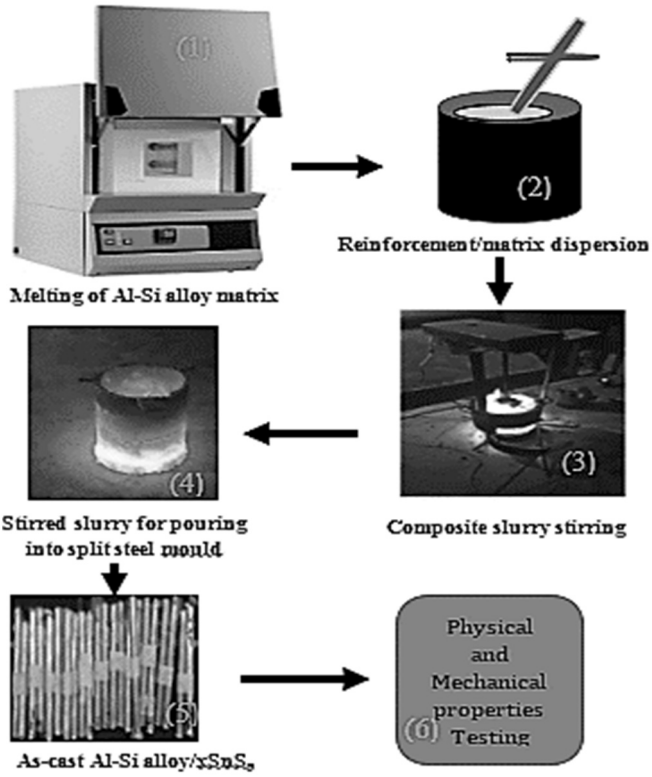


Figure 2. Illustrative pictures of Al-composite production process using stir-casting technique.

Physical, mechanical and morphology properties characterization

The Al-Si/xSnS_p composite obtained from stir-casting were evaluated by carry out physical, mechanical and morphological characterization.

Microstructural investigation of Al-Si/xSnS_p composites

The surface microstructural analysis of Al-Si alloy matrix and reinforced composite specimens were examined using Scanning Electron Microscope (SEM) Vega LMU from TESCAN Brno, Czech Republic incorporated with X-Act Energy Dispersive Spectroscopy (EDS) detector from Oxford Instruments, Oxford UK operated at 20kV accelerated voltage. Samples for SEM observation were prepared by cutting and machined down to ϕ8 mm by 4 mm height dimension and grinded up to 2000 grit size SiC paper in a sequence of 400, 800, 1200 and 2000 grits to produce a smooth shiny surface. The ground surface was then etched in 5 % nital solution before finally mounted on a SEM sample holder for morphological examination.

APTEFF, 51, 1-206 (2020) UDC: 693.9:669.713:629.33]:639.45+679.92
DOI: https://doi.org/10.2298/APT2051163K BIBLID: 1450-7188 (2020) 51, 163-180
BY-NC-ND
Original scientific paper

Density determination

Archimedes' principle as reported in the work of Usman et al., (12) was adopted to evaluate the density of Al-Si/xSnS_p composite and aluminium-silicon alloy. The weight of Al-Si/xSnS_p composite was firstly carried out in air as (w_a) on a digital electronic weighing (Kern;D-72336 Balingen, Germany) balance with serial number W1500761 and then immersed in graduated measuring cylinder to obtain the corresponding weight in water (w_l) equivalent to rise in volume. The weight in water was then taken and recorded to obtain the density of Al-Si/xSnS_p composite according to Equation 1.

$$\rho = \frac{w_a}{w_a - w_l} \quad [1]$$

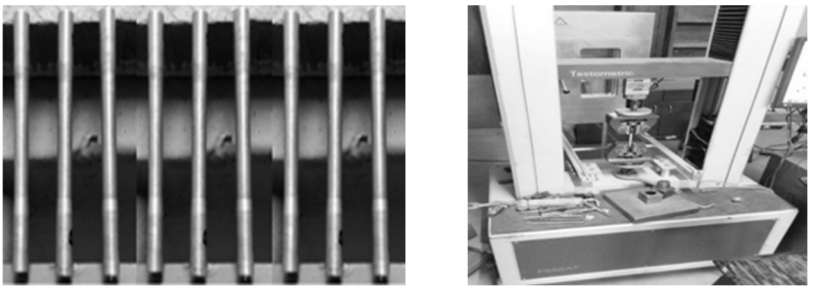
Where ρ = density (g/cm^3), w_a = weight in air and w_l = weight in water

Micro-hardness measurement

The hardness of the samples ground up to 1200 grit size at 400, 800 and 1200 grit size order for smoothness and flatness was measured as per ASTM E384 – 17 using a micro-Vickers hardness tester under an applied load of 4.9 N for 10 s. A minimum of five readings were taken at different points on each sample and the averaged of the readings were recorded as the hardness value for the Al-Si/xSnS_p composite samples.

Evaluation of tensile and compressive strengths of Al-Si alloy/xSnS_p composite

The tensile test of both unreinforced and Al alloy/SnS_p composites specimen (Figure 3a) were carried out using computerized Testometric Universal UTM (TUE-C-500) model tensile machine (Figure 3b) by subjecting the specimen into a gradual applied tensile force at 10^{-3} s^{-1} until fracture occurred. The specimens were prepared as per ASTM E-8 standard strain rate (27, 28). The compressive strengths of Al-Si/xSnS_p composite samples were also examined in accordance with ASTM E9-09 standard procedure under 10^{-3} s^{-1} strain rate and specimen dimension kept constant at 2.0 length to diameter ratio.



(a) (b)

Figure 3. Mechanical testing: (a) tensile samples and (b) tensile testing process

APTEFF, 51, 1-206 (2020) UDC: 693.9:669.713:629.33]:639.45+679.92
DOI: https://doi.org/10.2298/APT2051163K BIBLID: 1450-7188 (2020) 51, 163-180
BY-NC-ND
Original scientific paper

Impact strength determination

The impact strength of the Al-Si/xSnS_p composite was performed following ASTMD 256-93 standard using Avery Dension Universal Izod Impact – Testing machine, model number 6705U/33122 (18). The prepared samples (75×10×10 mm) of both un-reinforced and reinforced alloy samples was conducted on notched samples at depth of 2 mm in the middle and a notch tip radius of 0.25 mm at an angle of 45°. The striking hammer was raised to the maximum height and release freely to fall from gravity on the already clamped specimen and the readings of absorbed energy to fracture the samples were taken.

RESULTS AND DISCUSSION

Fourier Transform Infrared (TIR) analysis of reinforcement material

The Fourier Transform Infrared (FTIR) patterns of both calcined and uncalcined *Archachatina marginata* snail shell powders were as illustrated in Figure 4. This test was carried out to identify the functional group and phase composition of both the calcined and un-calcined SnS_p samples. The FTIR of un-calcined SnS_p contains mainly aragonite, calcite ($CaCO_3$), carbonate (CO_3^-) group with characteristic intensity peaks at 1452, 849.802 and 1799 (cm^{-1}) wavelengths respectively. A small peak of $Ca(OH)_2$ absorption functional group was also observed at 667 cm^{-1} (29). On the other hands, the calcined SnS_p depicts the characteristics IR bands at 1416 and 866 cm^{-1} intensity. These peaks correspond to CaO formation which is in line with the work of Loy et al. (29). In addition, a sharp peak of $Ca(OH)_2$ absorption was noticed with calcined SnS_p sample at 3644.26 cm^{-1} (29, 39). This may be attributed to high reactivity and affinity for moisture of CaO as a result of its hygroscopic nature when exposed at the time of characterization (30). Figure 5 was a plot of intensity against angle (2theta) for the XRD analysis of calcined and un-calcined SnS_p. The Figure shows uncalcined snail shell powders were characterized with many peaks unlike the calcined form which shows a well crystalized and scanty peaks. This implies that, uncalcined SnS_p has more phases than the calcined form with mono detectable phase. The main phase identified in un-calcined SnS_p sample occurs at diffraction peaks (26.27, 36.20, 37.9, 38.56, 45.91, 48.48, 50.2, 52.4)° corresponding to aragonite according to JCPDS 00-041-1475 reference code. Meanwhile, the main phase of calcined SnS_p sample occurs at diffraction peaks (32.43, 37.49, 53.89 and 67.73) corresponding to calcia (CaO) according to JCPDS 00-037-1497 reference code. The result implies that untreated snail shell powder mainly contains calcium carbonate and its calcination yielded mainly calcium oxide as the resulting product of calcination process of SnS_p due to loss of volatile phases. The high proportion of CaO ceramic phase in calcined shell suggests African giant land snail shell as a potential alternative inexpensive source of reinforcement material in metal matrix composites. These results are in good agreement with FTIR results (Figure 4) which also confirmed the liberation of carbonate group for the formation of CaO.

APTEFF, 51, 1-206 (2020) UDC: 693.9:669.713:629.33]:639.45+679.92
DOI: https://doi.org/10.2298/APT2051163K BIBLID: 1450-7188 (2020) 51, 163-180
BY-NC-ND
Original scientific paper

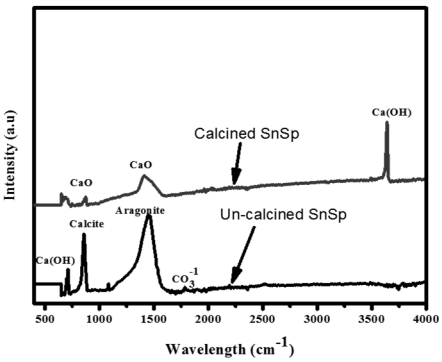


Figure 4. FTIR of calcined and un-calcined snail shell

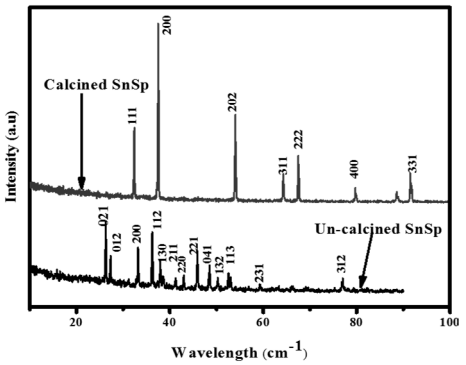


Figure 5. XRD graph of calcined and un-calcined snail shell

The morphology and particle size examination of calcined snail shell particulates used as reinforcement was as presented in Figure 6. It was observed that the calcined SnS particulates consist of particles of different sizes and shapes as a result of thermal necking and agitation of the calcination process. The minimum and maximum particle sizes as revealed by Gwyddion analysis were 0.219 μm and 2.009 μm respectively. The particles tend to disintegrate from larger particle size into smaller size through the process of diffusion into spheroid, oval, irregular quadrilateral shaped particles in fused form. Differences in colour of particles as depicted in the morphology were indication of heating effect of calcination process without any change in the compositional phases as indicated by XRD results.

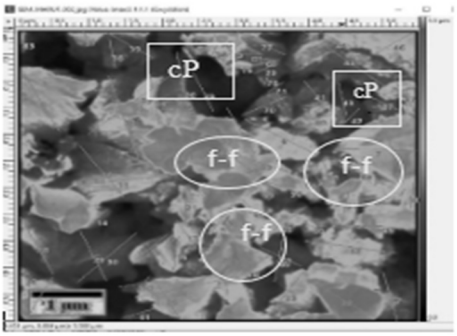


Figure 6. SEM morphology of calcined SnS powder

Density of aluminium-silicon/xSnS_p composites

Figure 7 is a graph of density variation of aluminium-silicon matrix reinforced with varying weight additions of calcined SnS_p and equivalent percentage density reduction in the composite produced. The graph shows decreasing trends in density of aluminium-silicon/SnS_p composite produced with increasing weight addition of SnS_p. The density of

APTEFF, 51, 1-206 (2020) UDC: 693.9:669.713:629.33]:639.45+679.92
DOI: https://doi.org/10.2298/APT2051163K BIBLID: 1450-7188 (2020) 51, 163-180
BY-NC-ND
Original scientific paper

unreinforced sample as presented in Figure 7 was 2.757gcm^{-3} and decreases with increasing addition of snail shell addition to 2.609 gcm^{-3} at 7.5 wt%. Quantitatively the addition of 7.5 wt% of SnS_p in aluminum-silicon alloy resulted in 5.37% density reduction in reinforced aluminium-silicon/SnS_p composite. The reduction in weight of composite produced could be attributed to the addition of light weight calcined snail shell powder as reported in our previous study which replaced the higher dense soft matrix phase alloy. Hence, addition of less dense and hard SnS_p can enhance the production of light weight composite material for improve performance. This result is in line with earlier reported works on metal matrix composites (31-35). Prasad *et al*. obtained a 2.4 % decrease in density with 8 wt% of rice husks while Shanmughasundaram *et al*. (32), reported 6.6 wt% density using flyash as reinforcement in aluminium composite and Usman *et al*. (12) recorded 19.9 % declined in density of bagasse reinforced aluminium matrix composite using double stir casting technique.

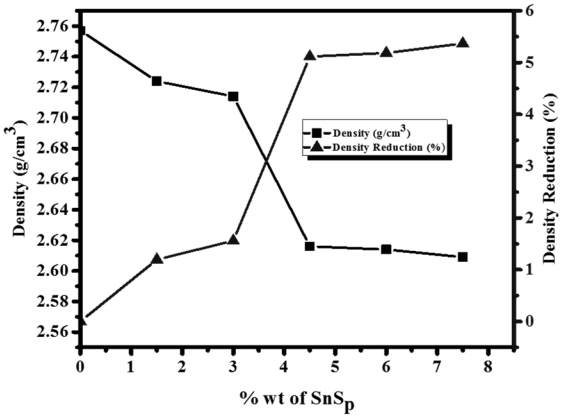


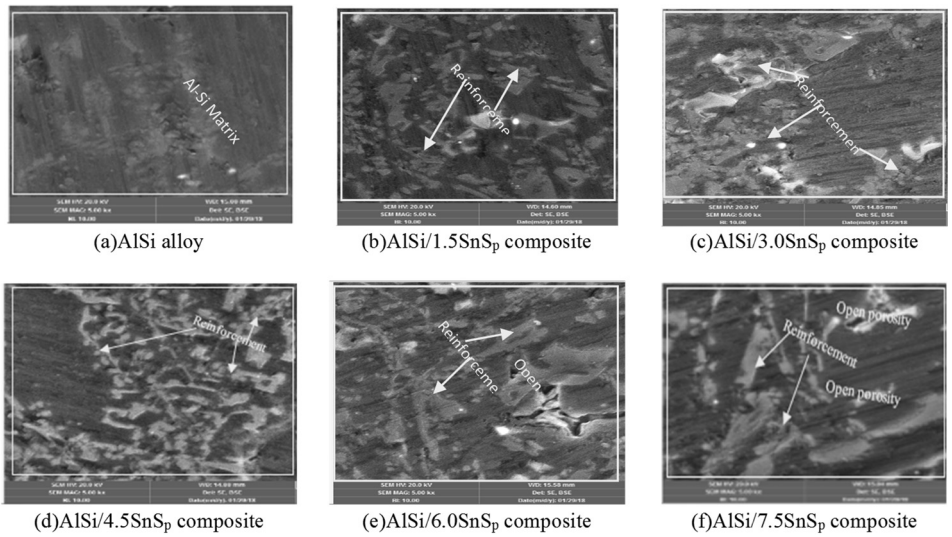
Figure 7. Density of Al-alloy/xSnS_p composite with wt% of SnS_p reinforcement.

Microstructure and chemical composition of Al-Si alloy/SnS_p composites

Figure 8 shows the microstructure and corresponding EDS analysis of SnS_p reinforced Al-Si alloy composites as obtained from scanning electron microscopy (SEM/EDS). The unreinforced aluminium alloy only shows a single phase with traces of silicon dendrites as discernible in the EDS micrograph. With 0.5 wt% SnS_p addition in Al-Si matrix, the calcium peak as shown in respective EDS result and as displayed in the microstructure appeared as separate phases (Figure 8b). This observation was similar to all microstructures obtained with varying weight addition of SnS_p (Figures 8c-f) in Al-matrix even though particle size of the matrix-reinforcement phases are becoming bigger given rise to spatial agglomeration and porosity inclusion within the Al-Si alloy matrix at 6 and 7.5 wt% of SnS_p addition. This could be due to high reactivity of calcium oxide and it's affinity for silicon at high temperature and as well as difficulty in stirring at high speed in such a condition. The addition of SnS_p is presumed to have enrich the dendritic strands of aluminium-silicon alloy in the unreinforced matrtix to forming calcium trioxo-silicate dendrite phase and aluminium-calcium phase particles which can act dislocation locker

APTEFF, 51, 1-206 (2020) UDC: 693.9:669.713:629.33]:639.45+679.92
DOI: https://doi.org/10.2298/APT2051163K BIBLID: 1450-7188 (2020) 51, 163-180
BY-NC-ND
Original scientific paper

for improve mechanical properties as evidenced in tensile, compressive and impact strengths of the composite produced. However, the open porosity as observed in in Figure 8e-f can be attributed to gradual drop in strengths of the composites. The EDS analysis of the respective alloy and composites as illustrated in Figure 8 and also provided in Table 2 as an attached file.



(a)AlSi alloy (b)AlSi/1.5SnS_p composite (c)AlSi/3.0SnS_p composite

(d)AlSi/4.5SnS_p composite (e)AlSi/6.0SnS_p composite (f)AlSi/7.5SnS_p composite

Figure 8. Microstructure of calcined snail shell at 0 – 7.5%wt (a-f) reinforced aluminium silicon alloys composites

Only aluminium, silicon and oxygen with no peaks of calcium or carbon was obtained in Figure 8a and Table 2. Addition of 1.5 wt% of SnS_p resulted in 0.6 wt% of calcium and as well as Al and Si as the main element in AlSi/1.5 SnS_p composite (see Table 2).

Table 2. EDS compsition of AlSi alloy and AlSi/xSnS_p composites

Composites	Al (wt%)	Std	Si (wt%)	Std	Ca (wt%)	Std	O (wt%)	Std	Od (wt%)	Std
Ao	87.15	0.85	7.70	0.01	0.00	0.00	4.85	0.50	0.30	0.00
A1	87.30	0.15	7.69	0.13	0.61	0.35	4.25	0.22	0.15	0.02
A2	87.05	1.25	7.65	0.63	1.20	0.48	3.88	0.2	0.22	0.00
A3	86.04	0.77	7.60	0.55	1.90	0.51	4.41	0.25	0.05	0.01
A4	87.90	0.50	7.30	1.02	1.80	0.46	2.36	0.18	0.64	0.01
A5	89.40	0.85	5.59	0.98	1.59	0.35	2.76	0.35	0.66	0.08

Od - other elements (C, Fe, Br, Na); Ao - AlSi alloy; A1 - AlSi/1.5SnS_p; A2 - AlSi/3.0SnS_p; A3 - AlSi/4.5SnS_p; A4 – AlSi/6.0 SnS_p and A5 – AlSi/7.5SnS_p

Further addition of SnS_p increase the peaks of calcium content in addition to Al, Si O_2 and other trace elements including carbon, iron, sodium and bromine of the resulting composites up to 4.5 wt% of SnS_p. However, above 4.5 wt% addition of SnS_p, a rapid fall

APTEFF, 51, 1-206 (2020)
DOI: https://doi.org/10.2298/APT2051163K
BY-NC-ND
UDC: 693.9:669.713:629.33]:639.45+679.92
BIBLID: 1450-7188 (2020) 51, 163-180
Original scientific paper

in calcium, silicon and oxygen peaks was observed in 6 and 7.5 wt% of SnS_p reinforced composites with the calcium peaks decreases to 1.80 and 1.59 wt% respectively in the resulting composites as discernible in Table 2. The presence of calcium peak (s) in the composites is an indication of presence of calcined snail shell particles in the aluminium matrix compared to un-reinforced alloy. The decrease in silicon, oxygen and calcium especially at higher calcined SnS_p addition, can be attributed to slag formation noticed at higher weight addition of SnS_p which may possibly coagulate out some of these elements along with the slag due to high reactivity. This factor might have been responsible for some decreases noticed in strength at higher percentage addition of SnS_p in Al-Si matrix composites.

Tensile fracture surface characteristics

Figure 9 shows SEM morphologies of the tensile fractured surfaces of unreinforced Al-Si alloy (Figure 9a) and reinforced Al-Si/xSnS_p composites samples (Figures 9b-f) respectively. The Figure shows a characteristic feature of cup and cone (cc), goose and dimples (gd) and as well as fibrous (F) morphologies in both the unreinforced and reinforced composites though with slight differences.

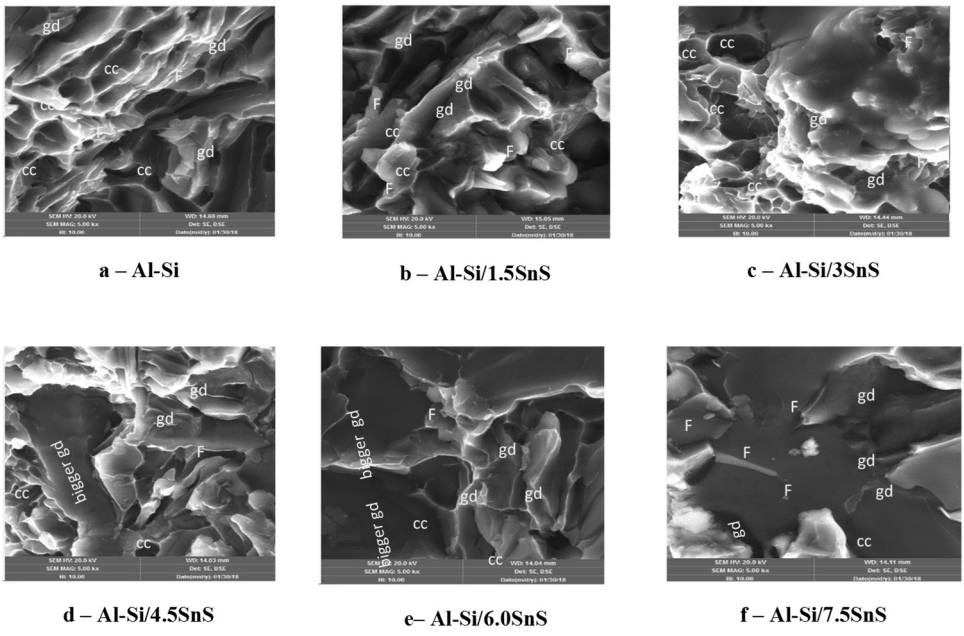


Figure 9. SEM of Al-Si composites' tensile fracture surfaces

These characteristic features imply a ductile failure mode in both un-reinforced and reinforced composites in which more energy can be absorbed before failure. However, increasing wt% addition of calcined SnS_p has no significant influence on the morpho-

APTEFF, 51, 1-206 (2020) UDC: 693.9:669.713:629.33]:639.45+679.92
DOI: https://doi.org/10.2298/APT2051163K BIBLID: 1450-7188 (2020) 51, 163-180
BY-NC-ND
Original scientific paper

logies but only results in gradual disappearance of the cone and cup structure into a large goose and dimple structure. This metamorphosis of structure with poor resistance to crack initiation tends to reduce the resilience of material to plastic deformation to pave way for sudden failure of the material. Hence gradual reduction in ductility of the composite may resulted with increasing addition of calcined SnS_p and as evidenced in percentage strain results in Figure 12.

Micro-hardness measurement

The hardness variation of control and Al-Si/xSnS_p composite produced with increasing weight percent addition of calcined snail shell was depicted in Figure 10. It was observed that the hardness increases with increasing weight percent of SnS_p for all reinforced Al-Si alloy. For instance, the hardness value of Al-Si alloy was 97.844 HV at 0 wt% and steadily increased to 118.02 HV at 6 wt% of SnS_p and then decreased to 108.36 HV at 7 wt% SnS_p addition. The increments in hardness results can be arrogated to an increase in weight percentage of hard ceramic phases of calcined SnS_p in aluminium alloy matrix. The calcined SnS_p contains phases like CaO, Fe_2O_3, Cr_2O_3 and remnant carbon of calcination process as revealed by XRD result (Figure 5). These phases are ceramics materials which are hard and rigid. Their presence in the Al-Si alloy matrix enhances composite phase hardness. Thus, resulting in strong bond interface between the matrix and reinforcement for increased hardness values in the produced composites (17, 33, 34). This is in accordance with the works of earlier authors (3, 12) and increase in composites hardness was linked to addition of hard ceramic reinforcement phase in the matrix. However, the slight decrement in hardness at 7.5 wt% could be as a result of removal of some hard phases (calcium) in form of slag due to high reactivity as noticed in SEM/EDS results.

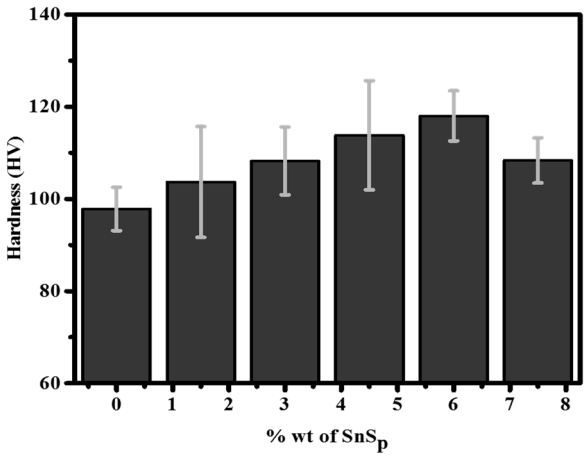


Figure 10. Influence of SnS_p wt% on hardness of Al-Si alloy/xSnS_p composite

APTEFF, 51, 1-206 (2020) UDC: 693.9:669.713:629.33]:639.45+679.92
DOI: https://doi.org/10.2298/APT2051163K BIBLID: 1450-7188 (2020) 51, 163-180
BY-NC-ND
Original scientific paper

Tensile and compressive strengths behaviour of Al-Si alloy/xSnS_p composites

The tensile and compressive strengths of Al-Si alloy/xSnS_p composites produced by stir-casting technique are presented in Figures 11 and 12, respectively. Both strengths increase with increasing weight percent of SnS_p. For instance, the average tensile strength increases from 155 ±5 MPa at 0 wt% to 211± 4.8 MPa when 4.5 wt% of SnS_p was incorporated into Al-Si matrix. Addition of SnS_p beyond this range does not further increase tensile strength but only resulted in slight decrement by 5 MPa. This implies that a maximum of 36% tensile strength increment at 4.5 wt% SnS_p addition in Al-Si alloy was achieved. Also, it is worthy of noting that, 6 and 7.5 wt% addition of SnS_p yielded 32 and 28% in tensile enhancement respectively compared to unreinforced Al-Si alloy.

Similarly, the compressive strength (Figure 12) of the same Al-Si/SnS_p composites depicted similar pattern of the tensile strength behaviour. The compressive strength increased with increasing addition of SnS_p from 462 ± 22.30 MPa SnS_p with Al-Si alloy matrix up to a maximum strength of 551.748 ± 19.56 MPa at 6 wt% of SnS_p addition though with slight reduction in percentage elongation. Beyond this limit of addition, only resulted in compressive strength decrement. The equivalent compressive strength increment at 6 wt% of SnS_p was 19% relative to unreinforced Al-Si alloy. The increase in both tensile and compressive strength as noticed in Al-Si/SnS_p composites was attributed to addition of hard ceramic phase of snail shell particles in Al-Si alloy with no signs of agglomeration as illustrated Figure 8. The presence of this SnS_p in Al-Si matrix restricts the displacement of silicon in aluminium matrix phase. Thus, resulted in high dislocation density which in turn requires higher force for plastic deformation. Moreover, the improvement in both strengths can be attributed to strain hardening effect as a result of localized stress action of SnS_p particles at different points within the matrix coupled with good wettability of SnS_p preheated at 400 °C prior the addition into the Al-Si alloy. These results corroborate with the works of Hassan and Aigbodion, Dwivedi *et al*., Aigbodion and Hassan, Prasad and Ramma (3, 19, 33, 35), where the strength improvement of reinforced matrix was attributed to the presence of hard particles and higher dislocation density along the grains of the matrix alloy. However, beyond 4.5 and 6 wt% of SnSp inclusion in matrix, the tensile and compressive strengths decrease marginally as depicted in Figures 11 & 12 respectively. This was due to addition of calcined snail shell in Al-Si alloy phase exceeding the saturation limit thus resulting in mis-matching of reinforcement-matrix interface giving rise to reduced dislocation density. Hence, reduction in strength of the composite set-in as noticed in both tensile and compressive strengths (Figures 11 & 12). Similar results were obtained by earlier researchers where decrease in strength was attributed to poor uniform distribution of harder phase in matrix at higher content (19). Moreover, the magnitude of compressive strength presented in Figure 10 was found to be higher than that of the tensile strength (Figure 11) of the same Al-Si/SnS_p composites. This can be attributed to presence of some defects such as micropore, gas inclusion in which the tensile strengths are more sensitive to compared to compressive strength action as experienced during testing. This is because the opposite applied loads coming towards each other during compressive action of the testing tends to entangle the interatomic interface which will initially increase the dislocation density and must be overcome before deformation commences. Thus, higher compressive strength compared to tensile strength.

APTEFF, 51, 1-206 (2020) UDC: 693.9:669.713:629.33]:639.45+679.92
DOI: https://doi.org/10.2298/APT2051163K BIBLID: 1450-7188 (2020) 51, 163-180
BY-NC-ND
Original scientific paper

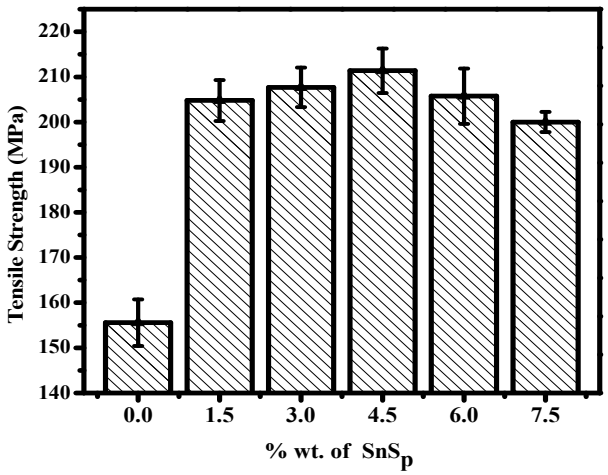


Figure 11. Influence of SnS_p wt% on tensile strength of Al-alloy/xSnS_p composite

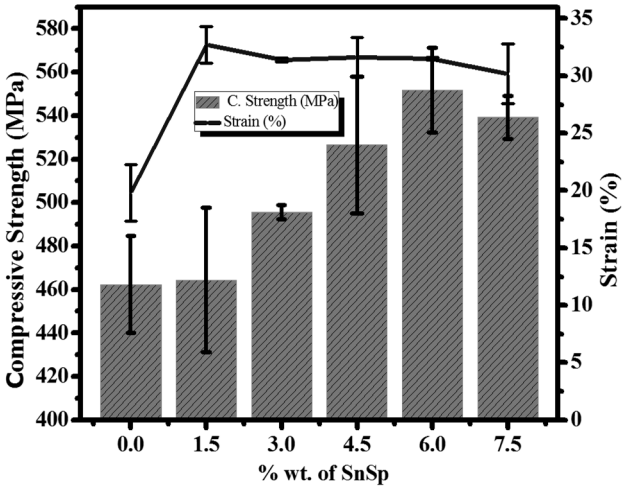


Figure 12. Influence of SnS_p wt% on compressive strength and strain of Al-alloy/xSnS_p composite

Influence of SnS_p addition on impact energy of Al-Si alloy

Figure 13 shows the impact energy of Al-Si alloy/xSnS_p composites. With increase in wt% of SnS_p addition in Al-Si matrix, the impact strength increases. As illustrated from Figure 13, the impact energy increased from 72.5 Joules at 0 wt% to 90.5 Joules when 7.5 wt% of SnS_p was dispersed in to the Al-Si alloy phase. The increment in impact strength obtained in Al-Si/7.0%SnS_p composite is equivalent to 25% when compare to un-reinforced Al-Si alloy. It was noticed that, this result looks contrary to some earlier reported

APTEFF, 51, 1-206 (2020) UDC: 693.9:669.713:629.33]:639.45+679.92
DOI: https://doi.org/10.2298/APT2051163K BIBLID: 1450-7188 (2020) 51, 163-180
BY-NC-ND
Original scientific paper

work in that, increasing addition of hard brittle reinforcement in metal matrix resulted into corresponding decrease in impact strength due to loss of ductility (3, 36). However, it will be noticed from the present work that, with addition of 1.5 wt% of calcined snail shell in the matrix, the percentage strain of the composite increases from 20% for the control sample to 30% plus which with further addition of reinforcement particles only result in slight reduction in strain. Therefore, the increase in impact energy as obtained in the study can be linked to good percentage strain property which damped the loading constraint and the rigidity of the calcined SnS_p second phase particles to hinder the composite impact deformation. This result was and follow the pattern reported in the work of Bello *et al*. and Abdullahi *et al.* (37, 38), where they reported increase in impact energy with increase in reinforcement addition in the matrix.

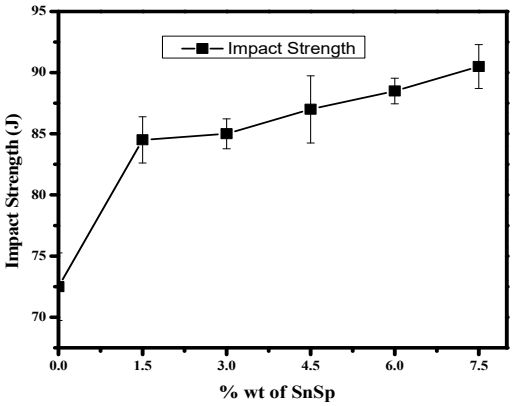


Figure13. Effect of SnS_p on impact strengths of Al- alloy/xSnS_p composite

CONCLUSIONS

From the results and discussion in this research work, the following conclusions are hereby submitted:

1. Calcined giant land snail shells particles were successfully incorporated as reinforcement material in aluminium-silicon scrap via stir casting technique.
2. Microstructural examination of the produced composites revealed a fair dispersion of SnS_p with high desolution in aluminum-silicon matrix with discernible aluminu-calcium-silicon dendrites, a major factor causing improvement in mechanical properties of Al-alloy/xSnS_p composites synthesized.
3. The dispersion of calcined SnS_p in Al-Si alloy matrix yielded a lighter and high impact energy in Al-Si/xSnS_p composite by 5.4 and 25 % respectively at 7.5 wt%. This implies that the developed composite can absorbed more energy before failure compared to un-reinforced Al-Si alloy.
4. The maximum tensile and compressive strengths obtained in as-cast Al-Si/xSnS_p composites were 211 ± 4.8 MPa and 552 ± 19.56 MPa at 4.5 wt% and 6.0 wt% SnS_p addition equivalent to 36 and 19% respectively relative to un-reinforced Al-Si8 alloy.

BY-NC-ND

The study concluded that calcined African giant land snail shell particulate can serves as an alternative low-cost reinforcement material in Al-Si alloy matrix for the production of lightweight with enhanced mechanical properties. The Al-Si/SnS_p composites can find application in the production of automotive components such as piston, connecting rods and cylinder lining.

Acknowledgements

The authors would like to acknowledge:
1. The financial assistance received from the Association of African University (AAU-small grants for theses and dissertation) towards this research work; and
2. The World Academy of Science (TWAS) and Interdisciplinary Research Centre in Biomedical Materials, COMSATS University Islamabad, Lahore Campus, Pakistan for Ph.D research fellowship and access to some of their Laboratory facilities.

REFERENCES

1. Lancaster, L.; Lung, M.H.; Sujan, D. Utilization of Agro-industrial wastes in metal matrix composites: Towards sustainability. *Waset 2013,* **2013,** 1136-1144.
2. Silva, M.J.; Kardoso, K.R.; Travessa, D.N. Production of NbC reinforced aluminium matrix composites by mechanical alloying. 21° CBECIMAT - Congresso Brasileiro de Engenharia e Ciência dos Materiais 09 a 13 de Novembro de 2014, Cuiabá, MT, Brasil, **2014,** *5738*(1), 2665–72.
3. Hassan, S.B.; Aigbodion, V.S. Effects of eggshell on the microstructures and properties of Al–Cu–Mg/eggshell particulate composites. *J King Saud Univ - Eng Sci*. **2015**, *27*(1), 49–56.
4. Kolawole1, M.Y.; Aweda, J.O.; AbdulKareem S. Archachatina marginata bioshells as reinforcement material in metal matrix composites. *Int J Automot Mech Eng.* **2017,** *14*(1), 4068–79.
5. Oghenevweta, J.E.; Aigbodion, V.S.; Nyiorm G.B.; Asuke F. Mechanical properties and microstructural analysis of Al–Si–Mg/carbonized maize stalk waste particulate composites. *J King Saud Univ - Eng Sci.* **2016**, *28*(2), 222–9.
6. Madakson, P.B.; Yawas, D.S.; Apasi A. Characterization of coconut shell ash for potential utilization in metal matrix composites for automotive applications. *Int J Eng Sci Technol.* **2012**, *4*(3), 1190–8.
7. Aigbodion, V.S.; Hassan, S.B. Effects of silicon carbide reinforcement on microstructure and properties of cast Al-Si-Fe/SiC particulate composites. *Mater Sci Eng A.* **2007**, *447*(1–2), 355–60.
8. Bodunrin, M.O.; Alaneme, K.K. Aluminium matrix hybrid composites: a review of reinforcement philosophies; mechanical, corrosion and tribological characteristics. *J Mater Res Technol.* **2015,** *4*(4), 434–45.
9. Kumar, G.B.V.; Rao, C.S.P; Selvaraj, N. Mechanical and tribological behavior of particulate reinforced aluminum metal matrix composites – a review. *J Miner Mater Charact Eng.* **2011,** *10*(01), 59–91.

BY-NC-ND

10. Miyajima, T.; Iwai, Y. Effects of reinforcements on sliding wear behavior of aluminum matrix composites. *Wear,* **2003,** *255*(1–6), 606–16.
11. Fatile, O.B.; Akinruli, I J. F.; Amori, A.A. Microstructure and mechanical behaviour of stir-cast al-mg-sl alloy matrix hybrid composite reinforced with corn cob ash and silicon carbide. *Int J Eng Technol Innov.* **2014**, *4*(4), 251–9.
12. Usman, A.M.; Raji, A.; Hassan, M. A.; Waziri, N.H. A comparative study on the properties of al-7 % si-rice husk ash and al-7 % si-bagasse ash composites produced by stir casting. *Int J Eng Sci.* **2014,** *3*(8), 1–7.
13. Khan, M.Z.; Anas, M.; Hussain, A.; Irshadul Haque, M.; Rasheed, K. Effect on mechanical properties of aluminium alloy composites on adding ash as reinforcement material. *J Met Mater Miner.* **2015**, *25*(2), 1–7.
14. Saravanan, S.D.; Kumar, M.S.; Effect of mechanical properties on rice husk ash reinforced aluminum alloy (AlSi10Mg) matrix composites. *Procedia Eng.* **2013**, *64*, 1505–13.
15. Alaneme, K.K.; Fatile, B.O.; Borode, J.O. Mechanical and corrosion behaviour of Zn-27Al based composites reinforced with groundnut shell ash and silicon carbide. *Tribol Ind*. **2014**, *36*(2), 195–203.
16. Singh, J.; Suri, N.M; Verma A. Affect of mechanical properties on groundnut shell ash reinforced Al6063. *Int J Technol Res Eng*. **2015,** *2*(11), 2347–4718.
17. Aku, S.Y.; Yawas, D.S.; Apasi, A. Evaluation of cast Al-Si-Fe alloy/coconut shell ash particulate composites. *Gazi Univ J Sci.* **2013**, *26*(3), 449–57.
18. Agunsoye, J.O.; Talabi, S.I.; Bello, S.A.; Awe, I.O. The effects of Cocos nucifera (coconut shell) on the mechanical and tribological properties of recycled waste aluminium can composites. *Tribol Ind.* **2014**, *36*(2), 155–62.
19. Dwivedi, S.P.; Sharma, S.; Mishra, R.K. Characterization of waste eggshells and $CaCO_3$ reinforced AA2014 green metal matrix composites: A green approach in the synthesis of composites. *Int J Precis Eng Manuf*. **2016**, *17*(10), 1383–93.
20. Jatto, E.O.; Asia, I.O.; Egbon, E.E; Otutu, J.O.; Chukwuedo, M.E; Ewansiha, C.J. Treatment of waste water from food industry using snail shell. *Acaedmia Arena*. **2010,** *2*(1), 32–6.
21. Aluko, F.A.; Adisa, A.A.; Taiwo, B.B.A.; Ogungbesan, A.M.; Awojobi, H.A. Quantitative measurements of two breeds of snail. *American Journal of Research Communication,* **2014**, *2*(5), 175–82.
22. Kant, S.; Singh, V. A. Stir casting process in particulate aluminium metal matrix composite: A review. I*nt J Mech Solids.* **2017**, *9*(1), 973–1881.
23. Babalola, P.O.; Bolu, C.A.; Inegbenebor, A.O.; Odunfa, K.M. Development of aluminium matrix composites: A review. *Online International Journal of Engineering and Technology Research,* **2014**, *2*, 1–11.
24. Sijo, M.T.; Jayadevan, K.R. Analysis of stir cast aluminium silicon carbide metal matrix composite: A comprehensive review. *Procedia Technol.* **2016**, *24*, 379–85.
25. Prasad, K.N.P.; Ramachandra, M. Effect of squeeze pressure on the hardness and wear resistance of Aluminium flyash composite manufactured by stir-squeeze casting. *Int J Eng Invent.* **2013**, *3*(4), 2278–7461.
26. Bhandare, R.G.; Sonawane, P.M. Preparation of aluminium matrix composite by using stir casting method. *Int J Eng Adv Technol.* **2013**, *3(*2), 61–5.

BY-NC-ND

27. Paul, K. K.; Sijo, M.T. Effect of stirrer parameter of stir casting on mechanical properties of aluminium silicon carbide composite. *Int. J. of Modern Eng. Res.* **2015**, *5*(August), 43–9.
28. Jain, S.; Rana, R.S.; Jain P. Study of microstructure and mechanical properties of Al- Cu metal matrix reinforced with b 4 c particles composite. *Int Res J Eng Technol.* **2016**;*3*(1):499–504.
29. Loy, C.W.; Matori, K.A.; Lim, W.F.; Schmid, S.; Zainuddin, N.; Wahab, Z.A. Effects of Calcination on the crystallography and nonbiogenic aragonite formation of Ark clam shell under ambient condition. *Adv Mater Sci Eng.* **2016**, *2016*, 1-8
30. Galván-Ruiz, M.; Hernández, J.; Baños, L.; Noriega-Montes, J.; Rodríguez-García, M.E.; Characterization of calcium carbonate, calcium oxide, and calcium hydroxide as starting point to the improvement of lime for their use in construction. *J Mater Civ Eng.* **2009**, *21*(11), 694–8.
31. Krishna, M.V.; Xavior, A.M. An investigation on the mechanical properties of hybrid metal matrix composites. *Procedia Eng.* **2014**, *97*, 918–24.
32. Shanmughasundaram, P.; Subramanian, R.; Prabhu, G. Some studies on aluminium - Fly ash composites fabricated by two step stir casting method. *Eur J Sci Res.* **2011**, *63*(2), 204–18.
33. Aigbodion, V.S.; Hassan, S.B. Experimental correlations between wear rate and wear parameter of Al-Cu-Mg/bagasse ash particulate composite. *Mater Des.* **2010**, *31*(4), 2177–80.
34. Rajan, T.P.D.; Pillai, R.M.; Pai, B.C.; Satyanarayana, K.G.; Rohatgi, P.K. Fabrication and characterisation of Al-7Si-0.35Mg/fly ash metal matrix composites processed by different stir casting routes. *Compos Sci Technol.* **2007,** *67*(15–16), 3369–77.
35. Prasad, D.S.; Krishna, A.R. Production and mechanical properties of A356.2/RHA composites. *Int J Adv Sci Technol.* **2011**, *33*, 51–8.
36. Alaneme, K.K.; Adama, S.I.; Oke, S.R. Mechanical properties and corrosion behaviour of ZN-27AL based composites reinforced with silicon carbide and bamboo leaf ash. *Leonardo Electron J Pract Technol.* **2014**, *13*(25), 58–71.
37. Bello S.A.; Agunsoye J.O.; Adebisi J.A.; Hassan S.B. Effect of aluminium particles on mechanical and morphological properties of epoxy nanocomposites. *Acta Period Technol.* **2017**, *48*, 25–38.
38. Abdullah, S.I.; Ansari, M.N.M. Mechanical properties of graphene oxide (GO)/ epoxy composites. *HBRC J.* **2015**, *11*(2), 151–6.

Received: 18 August 2020
Accepted: 5 October 2020